International Journal of Adhesion & Adhesives 122 (2023) 103334

Contents lists available at ScienceDirect

International Journal of Adhesion and Adhesives

journal homepage: www.elsevier.com/locate/ijadhadh

On the impact strength of adhesive bonded pin-and-collar joints

T.M. Brugo, D. Croccolo, M. De Agostinis *, S. Fini, G. Olmi, A. Zucchelli

Department of Industrial Engineering (DIN), University of Bologna, Viale del Risorgimento 2, 40136, Bologna, Italy

ARTICLE INFO

Keywords:
Epoxy adhesive
Anaerobic adhesive
Pin-and-Collar
Impact strength
Velocity
Strain rate

ABSTRACT

Nowadays, the adhesive technology is gaining relevance in industrial sectors where impact operating conditions are very common. At the same time, tests on cylindrical joints represent a well-established method for determining the static strength of structural adhesives. This work aims at assessing the impact properties of structural adhesives by means of cylindrical joints. The investigation involved two adhesive formulations (an epoxy resin and an anaerobic) and has been carried out under static, quasi-static and low-velocity impact conditions. The main outcomes of the work are: (i) the pin-collar specimen is well suited to analyzing the impact properties of adhesives; (ii) both adhesives showed a dependence of the strength and stiffness properties on the strain rate; (iii) the epoxy product showed a greater impact toughness than the anaerobic. In appendix, the authors report the tuning procedure of a CZM numerical model in a commercial FE package, based on the experimental results.

1. Introduction

Structural adhesives are widely used in industrial applications, due to a vast array of well-known favourable features, as reported in textbooks by da Silva et al. [1] and Adams et al. [2]. Nonetheless, a common characteristic of structural adhesives is their comparatively high sensitivity to the strain rate. As a general statement, adhesives' sensitivity to the strain rate means increased tensile and shear properties associated to a reduced fracture energy at high strain rates. In the past, such limitation hampered the adoption of structural adhesives in applications characterized by frequent impacts during the components' life [3]. In fact, polymeric materials, among which are included most adhesives, are known to display strain rate dependency, as reported by Lindholm [4]. Nowadays, the adhesive technology is gaining importance in industrial sectors where impact and bump are very common, as the automotive sector: due to that, extensive experimentation has been performed over the years to characterize the impact properties of several kinds of adhesives [5–7].

In the literature, two distinct approaches in impact testing of adhesives can be recognized: (i) bulk testing, aiming at isolating the response of the adhesive to impact loading – see da Silva et al. [8], (ii) testing of joints, in which other effects come into play, such as joint geometry, surface preparation, properties of the adherends (see You et al. [9], Blackman et al. [10], Beevers et al. [11] and Goglio et al. [12]). The latter approach is particularly suitable for assessing the combined influence of all the parameters that govern the joint strength, thus it is usually preferred for use in industrial applications. According to Adams [13], impact tests on adhesive joints may be further classified based on impact velocity: low ($v < 5$ m/s), medium (5 m/s $\leq v \leq 10$ m/s), high (above 10 m/s and usually up to 100 m/s). As a rule of thumb, one can assume that, in the case of low-velocity impacts, the problem can be treated as a vibrating system; in the medium-velocity range, strain and stress propagate as waves in the material, whereas in the high-velocity range the body (joint) collides with a body travelling faster than the sound velocity of the bodies [1]. Impact tests on adhesive joints can be performed according to different techniques: among others the Block Impact test [14,15], the Split Hopkinson Pressure Bar (SHPB) [5,16], the Drop-weight test, as reported by Maurel-Pantel et al. [7] and Vaidya et al. [17]. A literature survey reveals that the most widely adopted joint geometries for impact testing are Single and Double Lap Joints and Butt Joints, even if other configurations [6] have been explored by several authors.

In the last 15 years, following the steadily increasing demand for reliable and lightweight joints coming from the industry, Croccolo et al. devoted significant efforts to the characterization of cylindrical joints, by considering both purely adhesive joints [18] and hybrid-joints [19], investigating, among others, the static performance of mixed composite-metal hybrid joints [20], the fatigue performance of metal hybrid joints [21], the effect of the assembly process on the final strength of the joint [22], the thermal degradation of the adhesive [23]. Nonetheless, attentive examination of the literature reveals a comparatively small number of contributions dealing with the impact testing of cylindrical specimens. Among these, Bezemer et al. [24] used cylindrical

* Corresponding author.
E-mail address: m.deagostinis@unibo.it (M. De Agostinis).

https://doi.org/10.1016/j.ijadhadh.2023.103334
Received 13 June 2022; Received in revised form 1 December 2022; Accepted 30 January 2023
Available online 6 February 2023
0143-7496/© 2023 The Authors. Published by Elsevier Ltd. This is an open access article under the CC BY license (http://creativecommons.org/licenses/by/4.0/).

List of symbols:

A	Coupling surface [mm^2]
A_{min}	Minimum elongation at break [%]
D_C	Coupling diameter [mm]
D_{Se}	Pin external diameter [mm]
D_{Hi}	Collar internal diameter [mm]
D_{Se_AVG}	Pin external diameter – average of three measurements [mm]
D_{Hi_AVG}	Collar internal diameter – average of three measurements [mm]
E_a	Absorbed energy at a given time [J]
E_{am}	Average (calculated over the replicas) of the energy absorbed by the joint [J]
F_{Ad}	Decoupling force [N]
L_C	Coupling length [mm]
R_{e_min}	Minimum yield strength [MPa]
R_{m_min}	Minimum ultimate strength [MPa]
T_t^{max}	Maximum equivalent tangential contact stress [MPa]
g	Standard Earth gravity in [m/s^2]
m	Mass of the impactor [kg]
v_i	Impact velocity in [m/s]
$v(t)$	Impactor velocity at a given time in [m/s]
$\delta(t)$	Impactor displacement at a given time [m]
δ_t^c	Tangential slip at the completion of debonding [mm]
τ_{Ad}	Adhesive shear strength (averaged over the mating surface) [MPa]
ΔR	Radial clearance [mm]

List of Acronyms

SHPB	Split Hopkinson pressure Bar
ER	Engagement Ratio
SEM	Scanning Electron Microscope
FEA	Finite Element Analysis
CZM	Cohesive Zone Modelling

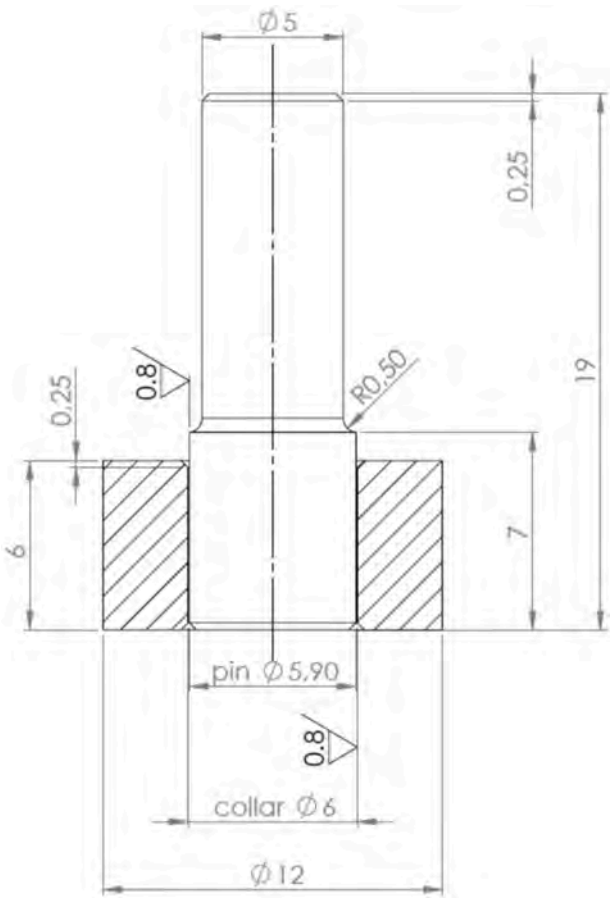

Fig. 1. Drawing of the specimen (not to scale).

specimens to load three different adhesives under shear: (i) Kommerling Korapur 649, a two-component polyurethane adhesive (PU); (ii) Araldit LY 5052, a two-component epoxy adhesive and (iii) Threebond 1132, an anaerobe sealing product, used with the Threebond Primer 3095C. The first is a tough adhesive whereas the second is a very brittle one. The third, an anaerobic adhesive, has its typical application in cylindrical joints. They investigated both the low-velocity and the high-velocity ranges, making use of a drop-weight machine and of an airgun respectively. They concluded that the pin-collar specimen is suitable for testing adhesive joints through the whole range of velocities, thus making it possible to directly compare their static and dynamic performance levels. Yokoyama [25] and Yokoyama and Shimizu [26] still made use of pin-and-collar specimens (bonded with a cyanoacrylate adhesive) but focusing on high-velocity impacts, carried out by means of a SHPB. They concluded that the combination between pin-collar specimens and SHPB allows measuring the shear strength of such joints up to stress rates in the order of 10^6 MPa/s but limited to metallic specimens. Engineering plastics, composites and rubbers cannot be tested on the same apparatus due to the large impedance mismatch between the Hopkinson bars and such comparatively soft materials. They observed that cyanoacrylate adhesive joints showed an increased shear strength at high strain-rates, also highlighting a significant effect of the following parameters of the joint: adhesive layer thickness and adherends material. Sawa et al. [27] tested pin-collar, epoxy bonded joints on a SHPB apparatus, assessing the effect of different adhesive thickness levels (0.1, 0.2 and 0.3 mm with a coupling diameter of 8 mm) and different stress rates (approximately $5\bullet10^5$–10^7 MPa/s). They found out that the strength of the tested epoxy adhesive displays a clear dependence on the stress rate, whereas the effect of the thickness parameter was less evident, suggesting the need to investigate broader thickness ranges.

Based on the outcomes of the literature survey, and with the aim of including the evaluation of impact loading scenarios in the assessment of cylindrical adhesive joints, the authors tested pin-collar joints like those used for standardized static tests [28,29] by adapting an existing drop-weight apparatus in service at the University of Bologna. The issues of novelty of the present investigation deal with: (i) direct comparison of two different adhesives (an epoxy resin and an anaerobic), under a range of low testing velocities of practical interest; (ii) assessment of the suitability of the pin-collar specimen geometry and test setup to evaluate the performance of the adhesive joint under a range of testing velocities.

Additionally, in the Appendix, the authors show the tuning process of a numerical CZM model in a commercial FE package (Ansys) based on the data retrieved by both the literature and the results of the present experimentation. This section may be useful to researchers and design engineers tasked with numerically simulating similar joints.

2. Materials and methods

2.1. Experimental tests

The specimen has been designed inspired from international

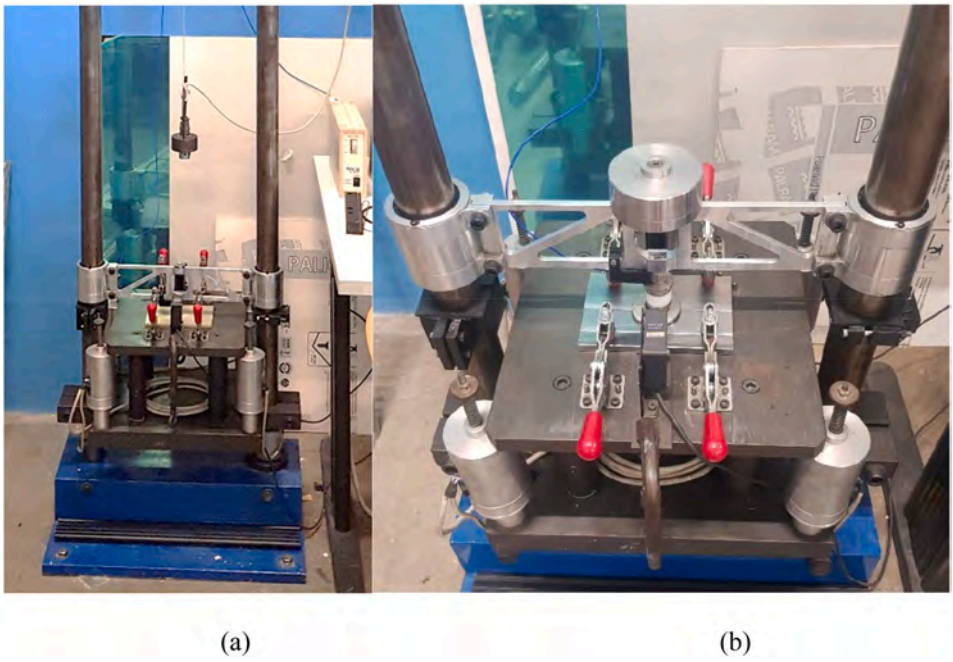

Fig. 2. Drop-weight test bench of the University of Bologna: (a) global view, (b) detail of the locking mechanism.

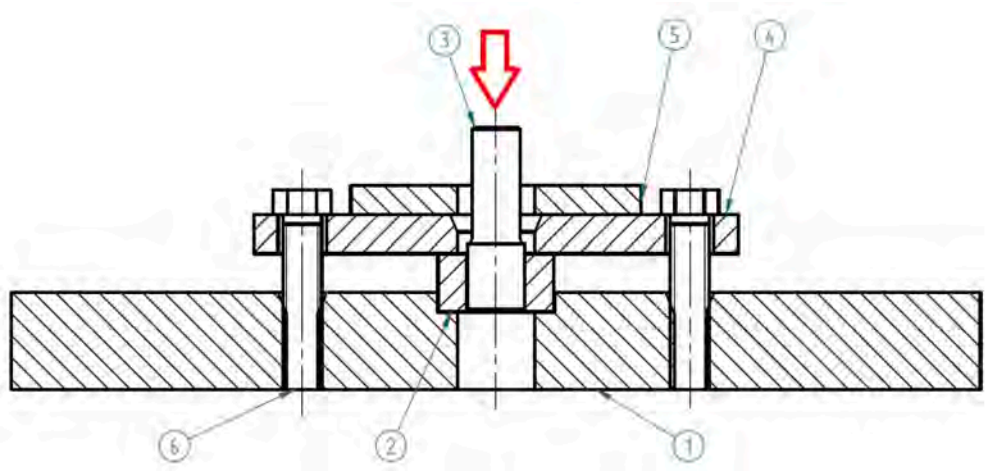

Fig. 3. Cross sectional view of the test fixture: (1) Plate, (2) Collar, (3) Pin, (4) Cover, (5) Rubber block, (6) M14 screw. The red arrow indicates the side of impact with the end-impactor (not to scale).

standards ISO 10123 [28] and ASTM D4562 – 01 [29]. Nonetheless, some adjustments had to be made to match the characteristics of the specific drop-weight apparatus used in the experiment. Particularly, the specimen had to be scaled down by a ratio of about ½ with respect to the standard sizes reported in Ref. [29]: the chosen coupling diameter is then $D_C = 6$ mm (see Fig. 1). The proportioning adopted for the pin and the collar turns into an Engagement Ratio ER ≈ 1 – see Croccolo et al. [18], quite close to that suggested by the standards (ER ≈ 0.90).

Pins and collars have been machined out of normalized C40 (steel number 1.0511) low carbon steel [30], cold drawn bars ($R_{e\ min} = 290$ MPa, $R_{m\ min} = 550$ MPa, $A_{min} = 17\%$). Two different adhesives have been tested:

(i) high strength, single component, anaerobic adhesive LOCTITE 648, specifically developed for cylindrical joints with or without interference [31];
(ii) bi-component, high strength epoxy adhesive LOCTITE Hysol 9466, characterized by a working life of 60 min (e.g., useful when re-positioning of the adherends is needed in the assembly line) [32].

Experimental tests have been performed at three different velocities: $3 \bullet 10^{-2}$ mm/s (static), $3 \bullet 10^{1}$ mm/s (quasi-static) and $3 \bullet 10^{3}$ mm/s (low-velocity impact). Such values have been chosen based on the needs of automotive manufacturers, and suitably spaced by setting them apart on the velocity axis by at least two orders of magnitude. For statistical evidence reasons, 5 Pin-And-Collar specimens (replicas) have been prepared for each kind of adhesive and for each velocity level to be tested, for a total population of 30. Static and quasi-static tests have been performed on a hydraulic universal test machine (Instron 8032), while low-velocity impacts have been carried out on a drop-weight test bench (Fig. 2), originally developed for testing laminate plates according to standard [33]. Such test bench is provided with a laser sensor which allows determining the impact speed, while the contact force is measured by a piezoelectric load cell (PCB 208C05), mounted on the tip of a hemispherical end impactor made of steel ($E = 200$ GPa, $\nu = 0.30$).

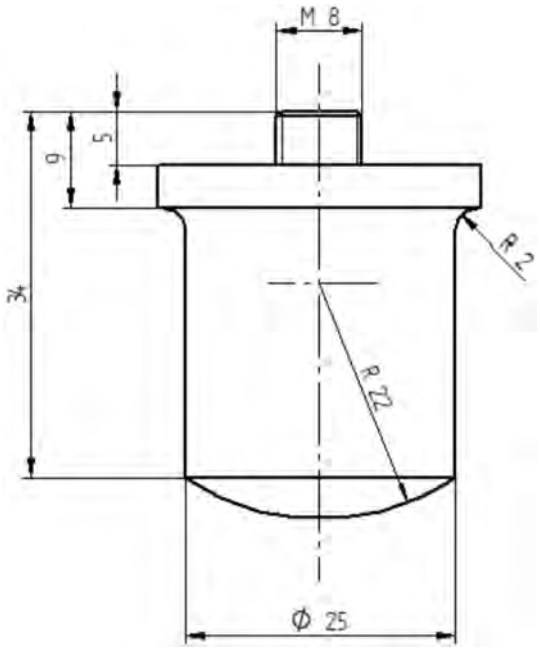

Fig. 4. Drawing of the end-impactor (not to scale).

The impactor is mounted on a sled made of EN AW 7075 T6 aluminium alloy, to which an additional steel weight is attached, in such a way that the total impact mass is about m = 2.57 kg. The dimensions of the impactor are much higher than those of the specimens, therefore it might be assumed as rigid. The maximum drop height is 3 m, which corresponds to a maximum theoretical impact energy of 76 J.

The force signal is sampled at a frequency of 10^5 Hz for a suitable duration to cover the whole impact event. Since the impact device can monitor the contact force and the impactor velocity just before impact, the velocity and displacement of the impactor can be calculated by single and double (numerical) integration operations, respectively [33]: the detailed procedure of this calculation may be found in Zarei et al. [34]. The energy absorbed during the impact is then calculated according to Eq. (1).

$$E_a(t) = \frac{m\left(v_i^2 - v(t)^2\right)}{2} + mg\delta(t) \quad (1)$$

where E_a (t) is the absorbed energy at a given time, m is the mass of the impactor in kg, v_i is the impact velocity in m/s, v(t) is the impactor velocity at a given time in m/s, g is the standard earth gravity in m/s^2 and δ(t) is the impactor displacement at a given time in m. Proper installation of the cylindrical test specimen on the drop-weight apparatus required the development of a suitable fixture, shown in Fig. 3, whereas a drawing of the end-impactor is reported in Fig. 4.

The experiment encompassed standard preliminary phases of dimensional control and cleaning [35], eventually followed by bonding of the specimens. All the pins have been initially measured by means of a micrometer (range 0–12 mm, accuracy 10^{-3} mm) to determine their diameters. The collars' hole diameters have been preliminarily checked by means of a 6 mm, H7 (−0 mm; +0.012 mm) go – no go gauge and then by a digital caliper (accuracy 10^{-2} mm). The axial length of the collar has been measured by means of the same caliper mentioned above. All the diametral dimensions have been averaged over three measurements made at equally spaced points along the circumference. In addition, pins P4 and P24 have been checked by means of a digital profilometer, retrieving an average roughness of R_a = 0.86 μm. Then, the samples have been arranged in pairs, to maintain the scattering of clearance within the values recommended by Refs. [31,32]. As for the anaerobic specimens, an average bonding area A = 111,7 ± 0.3 mm^2 and an average radial gap of ΔR = 0,050 ± 0.002 mm have been

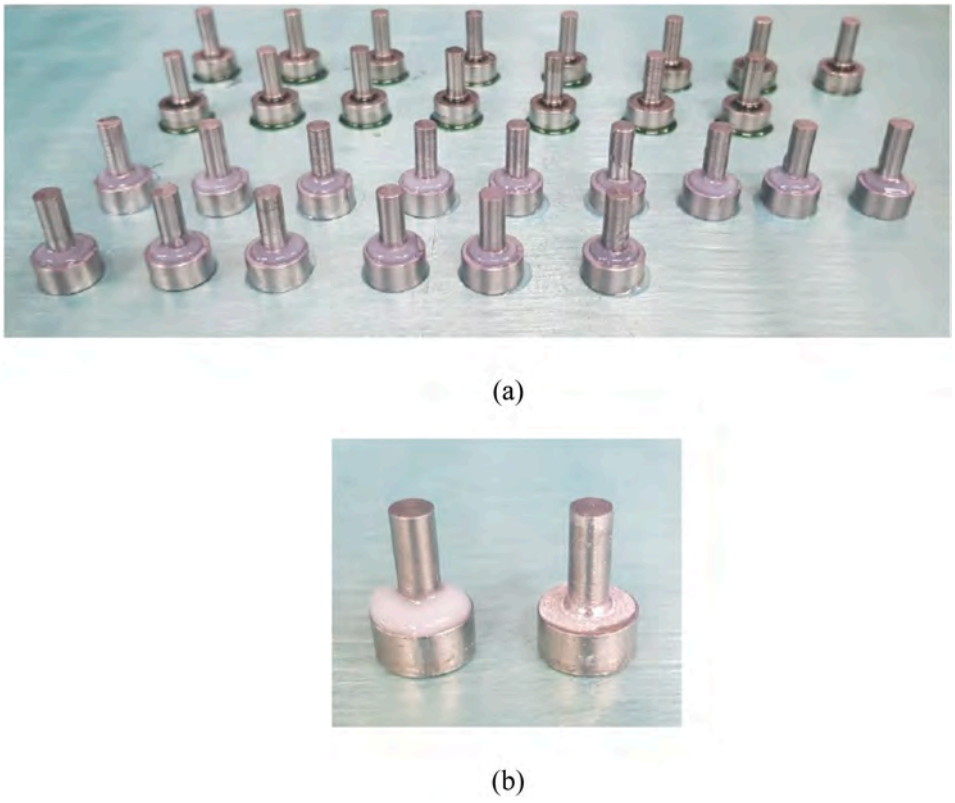

Fig. 5. Pin and collar specimens: (a) right after application of the adhesives – anaerobic bonds in the background and epoxy bonds in the foreground; (b) epoxy bonded specimen after polimerization, on the left and upon removal of the excess of adhesive, on the right.

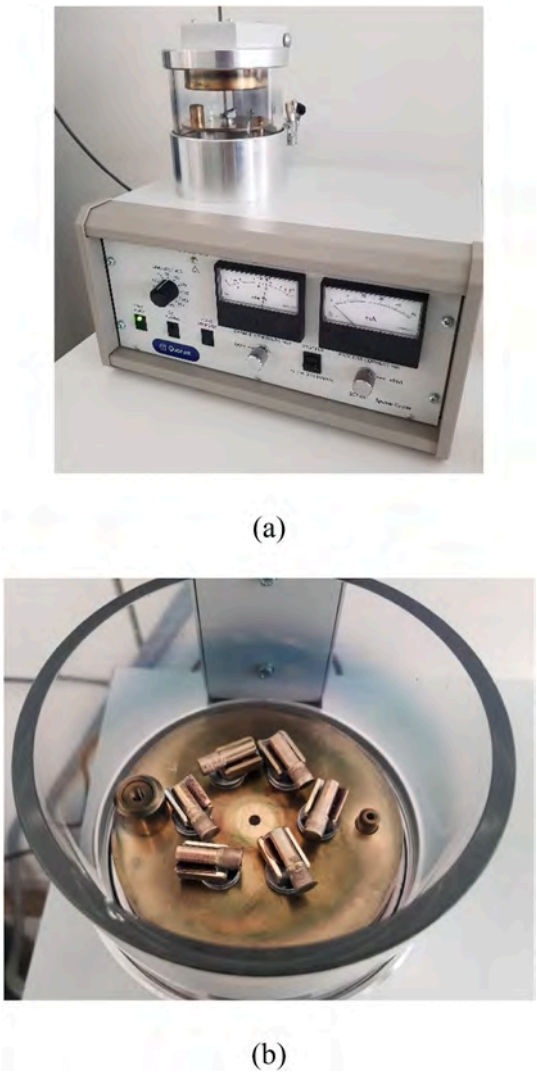

Fig. 6. (a) Sputter coating machine; (b) metallised surfaces of some pins right after sputter coating with gold.

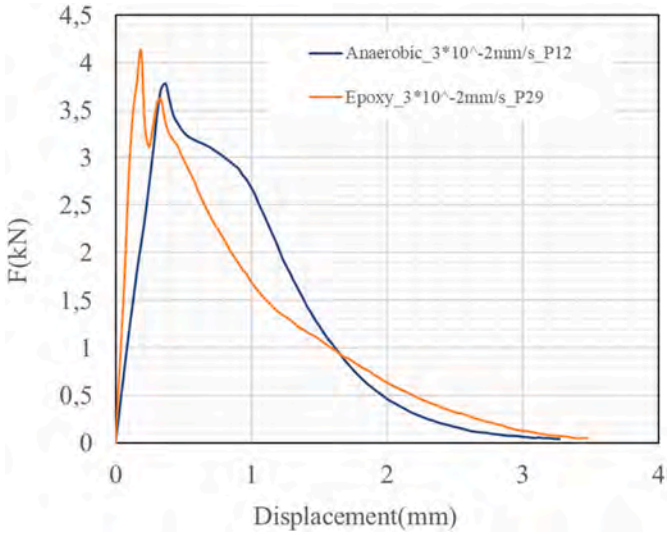

Fig. 7. Typical force – displacement diagram of a static test (v = 3•10^{-2} mm/s): anaerobic (blue curve) vs. epoxy (orange curve).

Table 1
Results of the static tests (stresses are averaged along the overlap).

Adhesive	F_m (kN)	F_{sd} (kN)	τ_m (MPa)	τ_{sd} (MPa)
Anaerobic	3.33	0.30	30.3	2.7
Epoxy	3.67	0.45	32.9	4.0

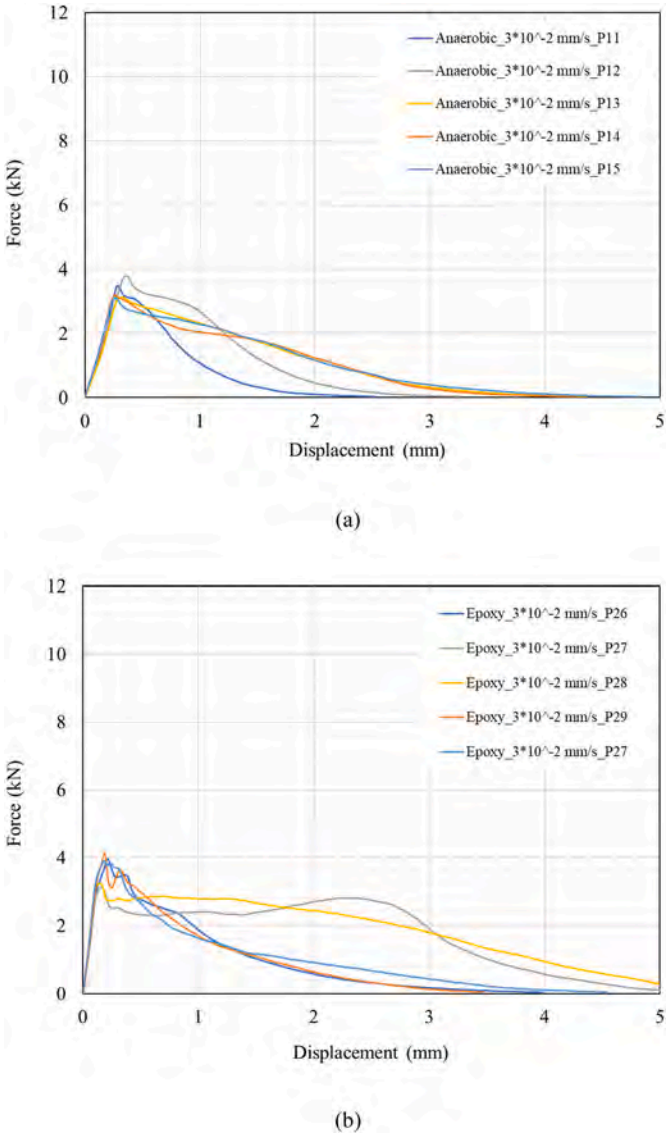

Fig. 8. Experimental Force-Displacement plots of the static test: (a) anaerobic, (b) epoxy.

obtained. In the case of epoxy specimens, an average bonding area A = 111,7 ± 0.3 mm^2 and an average radial gap of ΔR = 0,051 ± 0.004 mm have been obtained.

Cleaning operations have been carried out by means of a specific degreaser (Loctite 7063). Finally, the pins and the collars have been bonded, complying with the instructions provided by the adhesive manufacturer [31,32]. Once all the specimens have been bonded, they were left to polymerize at room temperature (RT = 20 °C) for a week, without changing their orientation (Fig. 5 (a)). In order to achieve the maximum strength of the joint, still following the lines of the adhesive manufacturer, the specimens have then been heated in an oven, at the following conditions: (i) 40 °C for 24 h for the anaerobic bonds, (ii) 80 °C for 30 min for the epoxy bonds. After that, the unpolymerized anaerobic

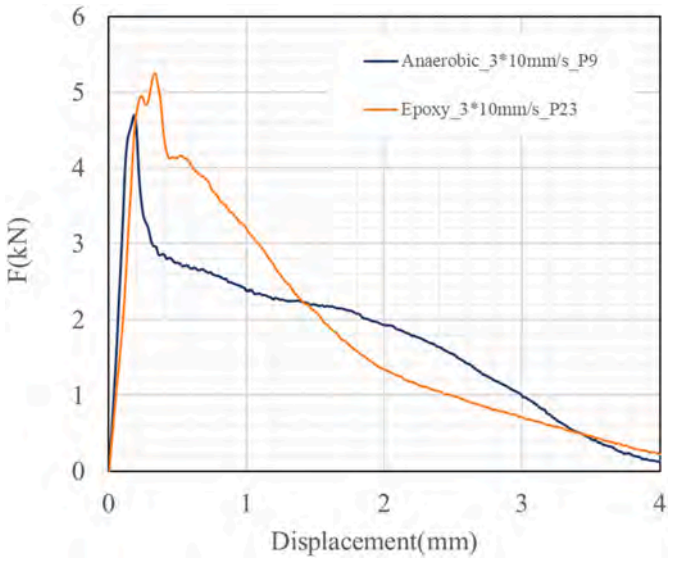

Fig. 9. Typical force – displacement diagram of a quasi-static test (v = $3\bullet10^{1}$ mm/s): anaerobic (blue curve) vs. epoxy (orange curve).

Table 2
Results of the quasi-static tests (stresses are averaged along the overlap).

Adhesive	F_m (kN)	F_{sd} (kN)	τ_m (MPa)	τ_{sd} (MPa)
Anaerobic	4.25	0.27	38.5	2.5
Epoxy	4.95	0.23	44.4	2.1

adhesive in excess has been removed by a cloth. On the contrary, epoxy-bonded specimens unavoidably display some polymerized adhesive at the re-entrant corner just outside of the coupling length. This excess of adhesive would have redistributed the stresses with respect to the theoretical condition, as reported in da Silva et al. [36,37], hence it has been accurately removed by means of a lathe running at slow speed (approximately 120 rpm): the result of this operation is shown in Fig. 5 (b). Lastly, some randomly chosen samples have been assessed with respect to their total runout to ensure coaxiality between the pin and the collar, thus the presence of a constant thickness layer.

After testing, all the fracture surfaces have been observed by means of an optical microscope (Zeiss Stemi 508) at approximately 10x magnification. The pins have also been observed by a scanning electron microscope (Phenom ProX). Due to the non-conductive nature of the residuals of adhesive on the surfaces of the specimens, observation has been enhanced by sputter coating, which is the standard method for preparing non-conducting or poorly conducting specimens prior to observation in a SEM. This process has been carried out by means of a sputter coater machine (Quorum Technologies, Laughton, UK, model SC7620), which allowed depositing a thin golden layer (about 10 nm thickness) over the fracture surface of the specimens: see Fig. 6 (a) and (b). Microscope observations allowed determining the failure mode (adhesive, cohesive or mixed) of each specimen, as well as assessing the correlation between the aspect of the fracture surface and the impact velocity.

3. Results

This section collects and analyzes all the data retrieved from the experimental tests, over three strain rates and for both types of adhesives. All stresses measured and reported in this section are calculated as average along the overlap area.

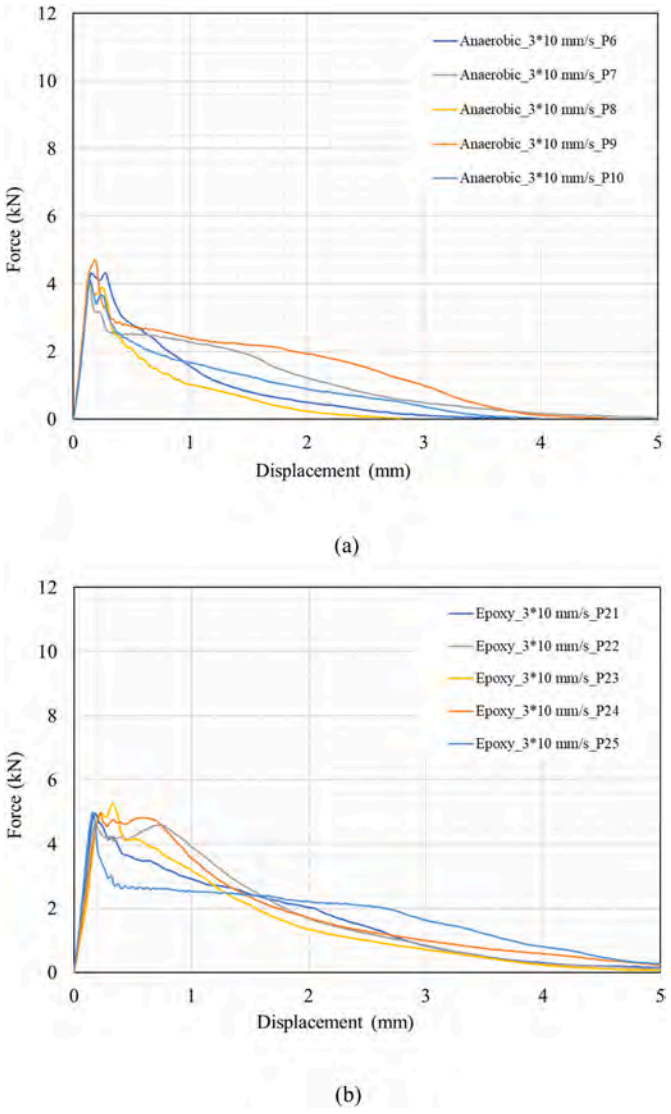

Fig. 10. Experimental Force-Displacement plots of the quasi-static test: (a) anaerobic, (b) epoxy.

3.1. Static tests

Fig. 7 shows the force – displacement trend obtained from a generic test on the hydraulic press, in the static test condition (v = $3\bullet10^{-2}$ mm/s). Although with slight differences in the numerical values, all the graphs obtained with this impact velocity share the trend illustrated in Fig. 7.

Looking at Fig. 7, it is possible to highlight slight differences in terms of static behaviour between the two adhesives. Firstly, the initial linear portion of the epoxy adhesive curve is characterized by a steeper slope, owing to its comparatively high stiffness with respect to that of the anaerobic, as reported in the literature by da Silva [1] and Öchsner [38]. Moreover, the shape of the curve beyond the peak of force is characterized by one or more rebounds in the case of the epoxy adhesive, probably related to a retention of adhesive debris at the interface, momentarily interlocking the pin and the collar even after the collapse of the bond (such outcome has been documented in the literature, e.g., see Croccolo et al. [23], Gallio et al. [39]). Results in terms of release forces (F_{ad}) and static strength values (τ_{ad}) of the two adhesives have been recorded and reported in Table 1, in terms of mean and standard deviation values (subscripts $_m$ and $_{sd}$, respectively).

As for the anaerobic samples, an average value of the release force

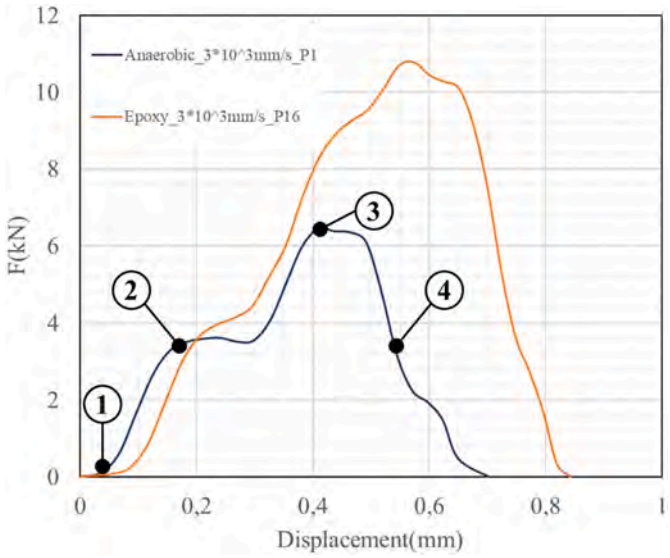

Fig. 11. Typical force – displacement diagram of a dynamic test (v = 3•10^3 mm/s): anaerobic (blue curve) vs. epoxy (orange curve).

Table 3
Results of the dynamic tests (stresses are averaged along the overlap).

Adhesive	F_m (kN)	F_{sd} (kN)	τ_m (MPa)	τ_{sd} (MPa)	E_{am} (J)	E_{asd} (J)
Anaerobic	6.69	0.30	59.5	2.7	2.30	0.19
Epoxy	10.76	0.21	96.2	2.0	4.55	0.09

F_m = 3.33 ± 0.30 kN, has been retrieved. Based on that figure, an average static shear strength τ_m = 30.3 ± 2.7 MPa can be calculated. Such result is in perfect agreement with the static shear strength measured by the adhesive manufacturer (31 MPa) for pin and collar samples polymerized for 7 days at 22 °C [31] and tested according to Ref. [28]. Tests carried out on the epoxy adhesive returned an average value of the release force F_m = 3.67 ± 0.45 kN. Based on that, an average static strength τ_m = 32.9 ± 4.0 MPa can be calculated. For the same epoxy adhesive, the manufacturer claims a static shear strength of 37 MPa [32], obtained on steel single-lap specimens in accordance with [40]. Finally, Fig. 8 ((a) anaerobic, (b) epoxy) shows the force-displacement curves obtained for all the specimens tested in the static condition.

3.2. Quasi-static tests

Fig. 9 shows the force – displacement trend obtained from a generic test on the hydraulic press, in the quasi-static test condition (3•10^1 mm/s). Although with slight differences in the numerical values, all the graphs obtained with this impact velocity share the trend illustrated in Fig. 9. The same remarks made for the static tests can be repeated for this load case, except the behaviour of the two adhesives in the linear portion of the force displacement curves. In fact, the quasi-static test reveals quite a different behaviour in terms of sensitivity of the stiffness with respect to the strain rate. Looking at Fig. 9, it can be noticed how the two linear portions are now almost coincident, in contrast to what shown in Fig. 7. This outcome will be clarified better in the discussion section. Experimental results are reported in Table 2.

As for the anaerobic samples, an average value of the release force F_m = 4.25 ± 0.27 kN, has been retrieved. Therefore, an average shear strength τ_m = 38.5 ± 2.5 MPa can be calculated. The epoxy adhesive showed an average value of the release force F_m = 4.95 ± 0.23 kN. Then, an average shear strength τ_m = 44.4 ± 2.1 MPa can be calculated. Finally, Fig. 10 ((a) anaerobic, (b) epoxy) shows the force-displacement curves obtained for all the specimens tested in the quasi-static condition.

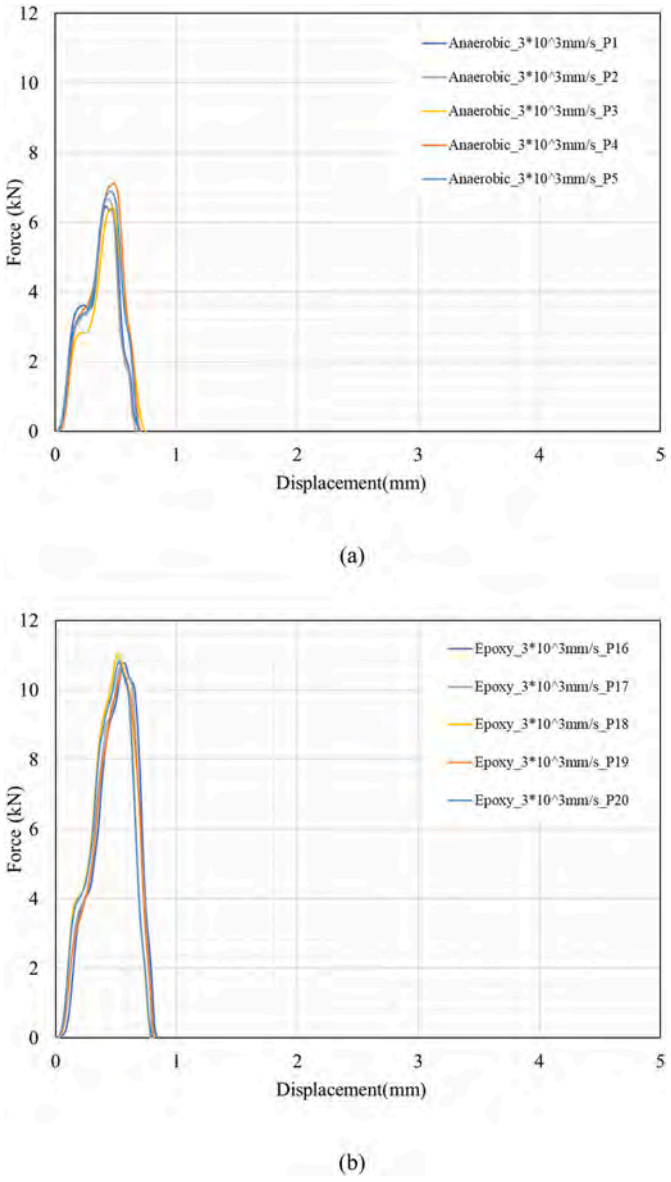

Fig. 12. Experimental Force-Displacement plots of the dynamic test: (a) anaerobic, (b) epoxy.

3.3. Dynamic tests

Fig. 11 shows the force – displacement trend obtained from a generic test on the drop-weight apparatus, corresponding to the dynamic test condition (3•10^3 mm/s). Although with slight differences in the numerical values, all the graphs obtained with this impact velocity share the trend illustrated in Fig. 11.

For the sake of clarity, some key features of the force-displacement curves obtained with this impact velocity have been indicated by balloons applied to the anaerobic adhesive curve in Fig. 11 and are here below summarised:

1. The end impactor comes into contact with the pin, and after an initial plateau, the force starts rising
2. Humps on the initial (pseudo-linear) portion of the curve, due to the excitation of the natural frequencies of the testing apparatus
3. Peak of force generated upon rupture of the adhesive layer
4. Sudden force decrease (expulsion of the pin).

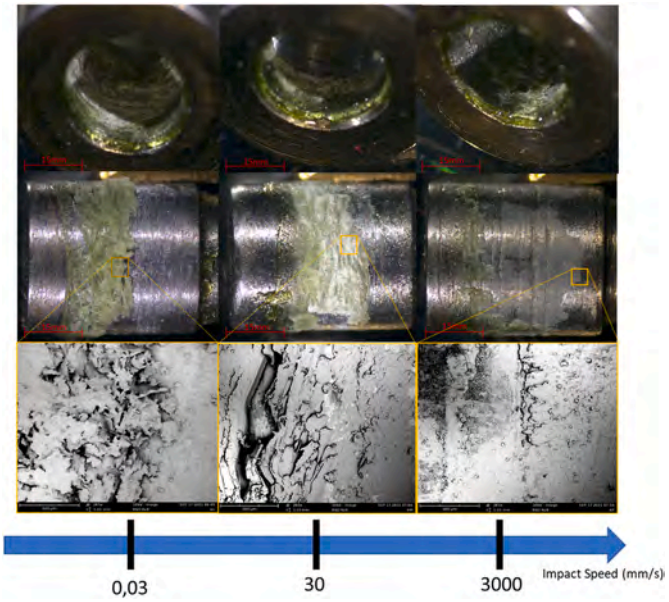

Fig. 13. Evolution of the fracture surface vs. impact velocity for anaerobic samples.

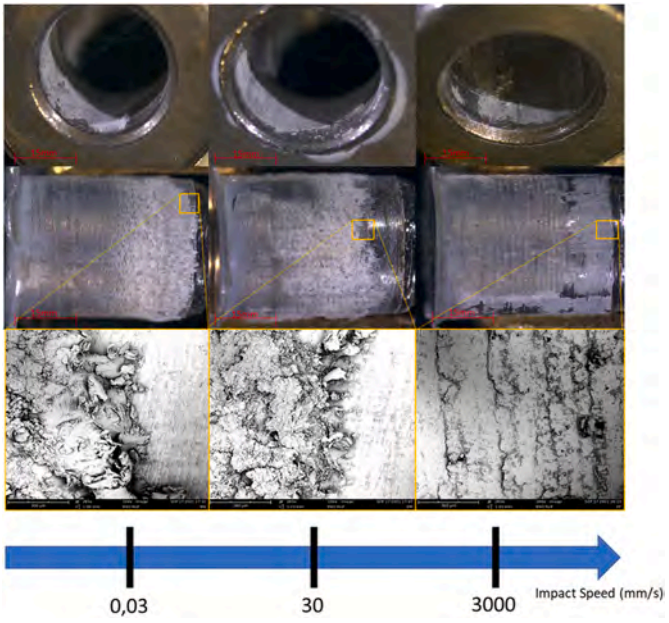

Fig. 14. Evolution of the fracture surface vs. impact velocity for epoxy samples.

Based on the results reported in Table 3, the following observations can be made. As for the anaerobic samples, an average value of the release force $F_m = 6.69 \pm 0.30$ kN has been retrieved. Therefore, an average shear strength $\tau_m = 59.5 \pm 2.7$ MPa can be calculated. The epoxy adhesive showed an average value of the release force $F_m = 10.76 \pm 0.21$ kN. Then, an average shear strength $\tau_m = 96.2 \pm 2.0$ MPa can be calculated. For both adhesives, the total energy absorbed by the sample has been calculated, according to Standard [33]. Anaerobic samples showed an $E_{am} = 2.30 \pm 0.19$ J, whereas Epoxies scored a higher value of $E_{am} = 4.55 \pm 0.09$ J. Finally, Fig. 12 ((a) anaerobic, (b) epoxy) shows the force-displacement curves obtained for all the specimens tested in the dynamic condition.

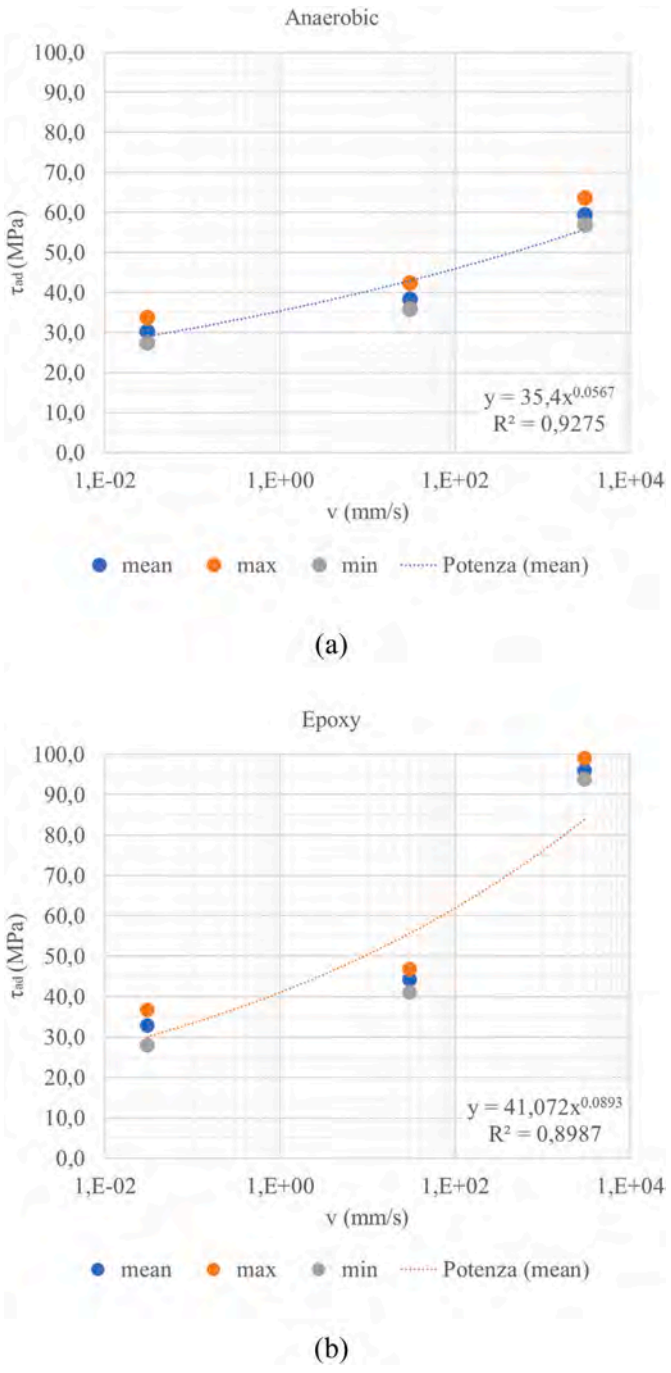

Fig. 15. Shear strength vs. impact velocity for: (a) anaerobic samples; (b) epoxy samples. Stresses are averaged along the overlap.

3.4. Microscope observation of the fracture surfaces

The outcomes of the microscope observations are summarised in Fig. 13 for the anaerobic samples and in Fig. 14 for the epoxy samples.

According to the evidence reported in the figures above, the following conclusions may be drawn: (i) failure is of the cohesive type for all observed specimens; (ii) both adhesives display a clear transition between a ductile failure towards a fragile failure for increasing impact velocities. Such behaviour can be better appreciated by attentively examining the SEM images reported on the last row of each figure.

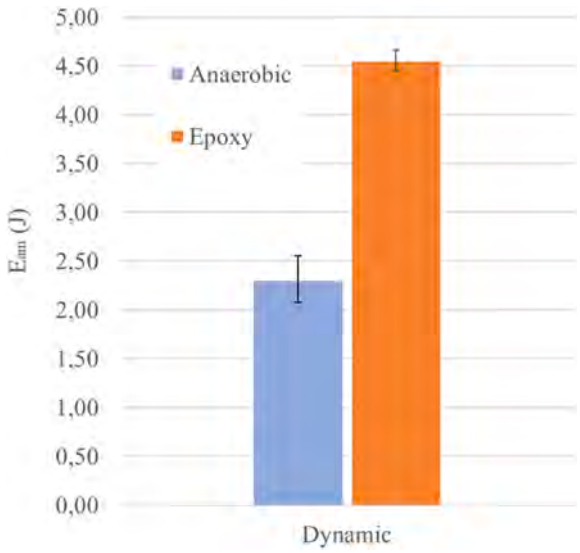

Fig. 16. Comparison of the absorbed energies (anaerobic vs. epoxy) in the dynamic test conditions.

4. Discussion

Static tests returned shear strength values well in accordance with those reported by the adhesive manufacturer, in both cases. Based on that outcome, the authors concluded that the specimen was able to provide a suitable mechanical strength (at least in the static condition), hence excluding any major deficiencies affecting the bonding process, which might affect the following dynamic tests.

By looking at Fig. 15, it is possible to observe the different behaviour of the two adhesives at increasingly high impact velocities. Although in the static test conditions, the two adhesives display similar strengths, the epoxy is characterized by a marked strain-rate strengthening behaviour. This outcome can be better appreciated by considering the second-order polynomial interpolations of the mean strength values proposed in both Fig. 15 (a) and (b): the interpolating function relevant to the epoxy adhesive is characterized by a greater derivative with respect to the impact velocity.

Analysis of the mean absorbed energy values (Fig. 16) confirms the favourable behaviour of the epoxy adhesive, in contrast to that of the anaerobic.

Attentive analysis of the experimental data, in terms of force – displacement plots (Fig. 17), leads to drawing one more interesting conclusion: while the epoxy adhesive does not undergo any strain-rate stiffening (Fig. 17 (a)), the anaerobic product shows a sharp increase in stiffness when the impact velocity shifts from $3 \bullet 10^{-2}$ mm/s (static) to $3 \bullet 10^{1}$ mm/s (quasi-static), with a ratio between the quasi-static and static stiffnesses of approximately 2.6 (see Fig. 17 (b)).

Such different behaviours are well in agreement with the literature: Goglio et al. [5] noticed little difference between the static and dynamic stiffness of an epoxy adhesive, whereas careful analysis of the data provided by Bezemer et al. [24] suggests an opposite behaviour of anaerobic adhesives. Moreover, such differences further justify the comparatively favourable behaviour of the epoxy adhesive when the impact velocity increases.

5. Conclusions

This work analyzed the effect of impact loading on cylindrical adhesive joints, making use of pin-collar joints like those used for standardized static tests. The investigation involved two different adhesives (an epoxy resin and an anaerobic) and comprises an experimental comparison between their static (0,03 mm/s), quasi-static (30 mm/s) and low-velocity (3 m/s) impact strength. The main outcomes of the work can be summarised as follows: (i) the pin-collar specimen is well suited to analysing the impact properties of adhesives, as well as it allows direct comparison to their static strength evaluated according to well-established international standards; (ii) both adhesives shown a strain-rate strengthening effect, whereas only the anaerobic product displayed a strain-rate stiffening effect; (iii) the epoxy product showed a better performance (greater toughness) than the anaerobic for increasing impact velocities.

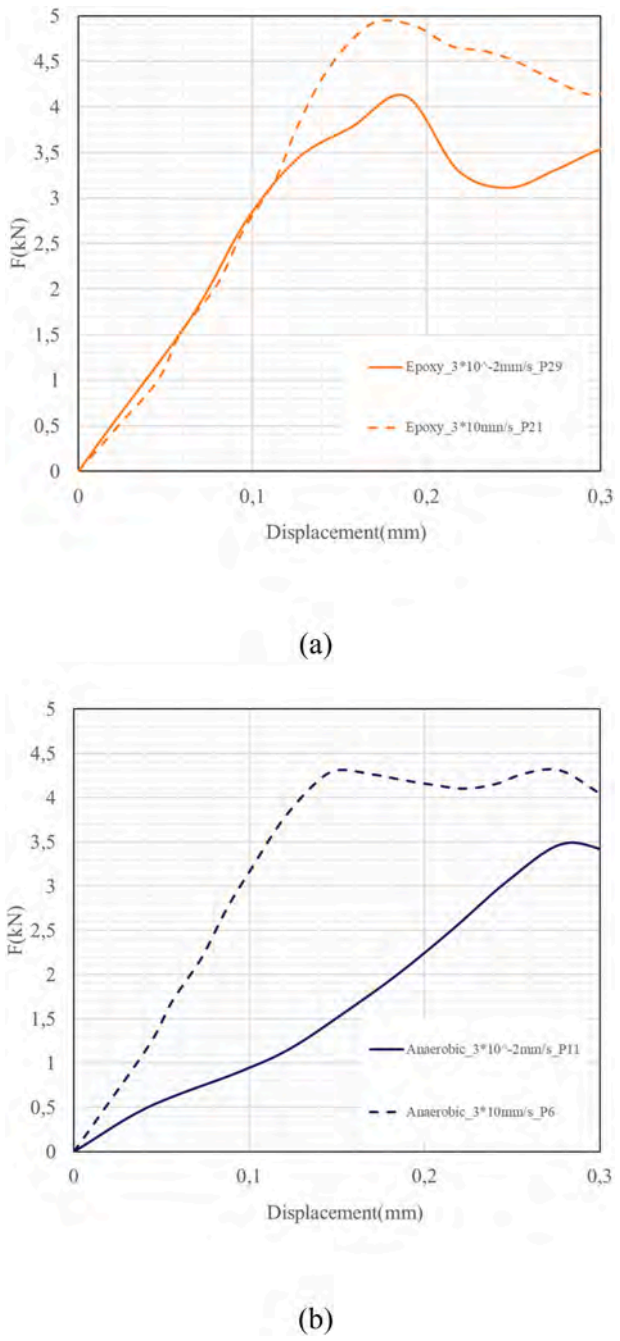

Fig. 17. Comparison between the slopes of the first portion of the force – displacement curve for (a) epoxy and (b) anaerobic adhesives, as a function of the impact velocity.

Declaration of competing interest

The authors declare the following financial interests/personal

relationships which may be considered as potential competing interests: Massimiliano De Agostinis reports equipment, drugs, or supplies was provided by Henkel Italy Srl.

Data availability

Data will be made available on request.

Acknowledgements

The authors gratefully acknowledge Mr. Simone Zanetti, TCS Application Engineer, General, Manufacturing & Maintenance, Educational at Henkel Italia S.r.l. for providing the adhesives for this experimentation. The contribution of thesis student Mr. Giulio Ravagli is also gratefully acknowledged.

Appendix A. numerical analysis

In order to provide researchers and design engineers with a practical example of the numerical assessment the impact strength of cylindrical joints by means of a commercial package, finite element analyses (FEA) have been performed by means of Ansys® 19.2 and by exploiting the Cohesive Zone Modelling (CZM) [41–43], combined with a non-linear implicit analysis solved by the Newton Rapson method. The CZM properties have been tuned up based on the outcomes of both the experimental outcomes of this research and the data reported in the literature for similar adhesives (e.g., see Pirondi et al. [44] and Campilho et al. [45]).

The problem is axisymmetric in nature; hence it has been modelled by 2D axisymmetric elements and imposing the following boundary conditions: (i) the collar has been constrained by restraining the displacement of its bottom face along the axial direction (y); (ii) a displacement along the axial direction (y), was imposed to the upper face of the pin, according to the experimental results. Both adherends have been discretized by second order (8-node) axisymmetric quadrilateral plane elements (PLANE183 in the Ansys nomenclature). The CZM interface between the two adherends has been modelled by bonded contact elements (CONTA172 with Pure penalty formulation, Asymmetric behaviour, small sliding set to OFF), through which the interfacial separation is defined in terms of contact gap and tangential slip distance. A bilinear CZM traction separation law, based on the model proposed by Alfano and Crisfield [46], have been used to represent the adhesive debonding behaviour in pure mode II (shear), because the tangential slip dominates the separation behaviour, due to the axial symmetric geometry and loading condition.

Although the numerical analysis herein reported is not a dynamic simulation (inertial effects are not considered), the solution steps have been defined in terms of time instead of divisions, in order to have full control of the artificial viscous damping of the CZM debonding parameter, which is expressed in units of time. Indeed, as recommended by the Ansys guidelines, the artificial damping coefficient should be smaller than the minimum timestep size, so that the CZM traction separation behaviour is not affected by it. The complete duration of the nonlinear analysis has been artificially set to 1 s, with a timestep set to 10^{-2} s, in order to correctly catch the evolution of stresses and strains over time, and an artificial damping coefficient set to 10^{-3} s (i.e., one order of magnitude smaller than the timestep).

The adherends have been discretized by a grid mesh (face meshing), refined towards the overlap edges in the axial and radial directions (edge sizing bias factor set to 5), in order to capture the high stress gradient which develops at the free edges [23]. The average element edge size has been set to 0.2 mm. A mesh study on the influence of the CZM element dimension on the accuracy of the simulation was performed. The average cohesive element edge dimension was varied between 1 mm and 0.02 mm, keeping the bias factor set to 5. In Fig. 18, the joint strength (F_{ad}^{FEM}) normalized to the average strength of all the simulations with different sizes ($F_{ad\ avg}^{FEM}$) is plotted vs the average CZM element edge dimension. The graph shows a negligible influence of the mesh size lower than 1 mm on the adhesive strength prediction of the pin collar joint. This can be ascribed to the length of the cohesive zone, defined as the distance from the crack tip to the point where the maximum cohesive traction is attained. As observed in the following (see Fig. 21 (c)), the maximum tangential stress is distributed along a wide zone that covers most of the bond length and for at least 5 mm. This is due to the loading condition (mode II) and comparatively high stiffness of the adherents with respect to the adhesive. Turon et al. [47] and Harper et al. [48] suggest that at least 3 elements are needed to accurately represent the tangential stress developed ahead of the crack tip and to predict the propagation of delamination, which correspond to an element dimension smaller than 1.67 mm in the present case. Such prescription is in perfect agreement with the choice made herein.

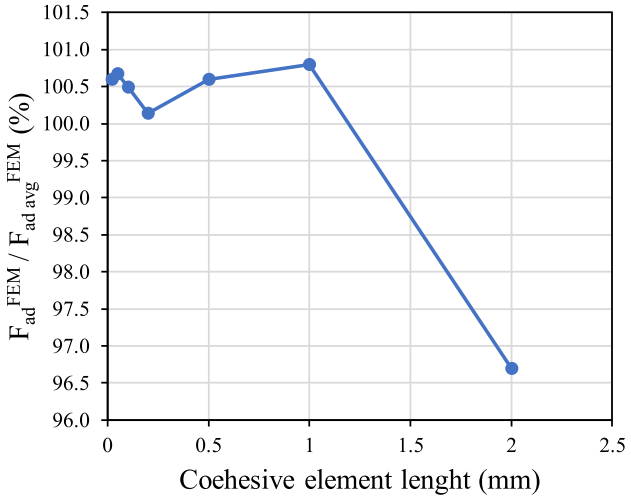

Fig. 18. Convergence analysis for the choice of the cohesive element length.

A detail of the boundary conditions (Fig. 19 (a)) and of the meshed model (Fig. 19 (b)) is shown below.

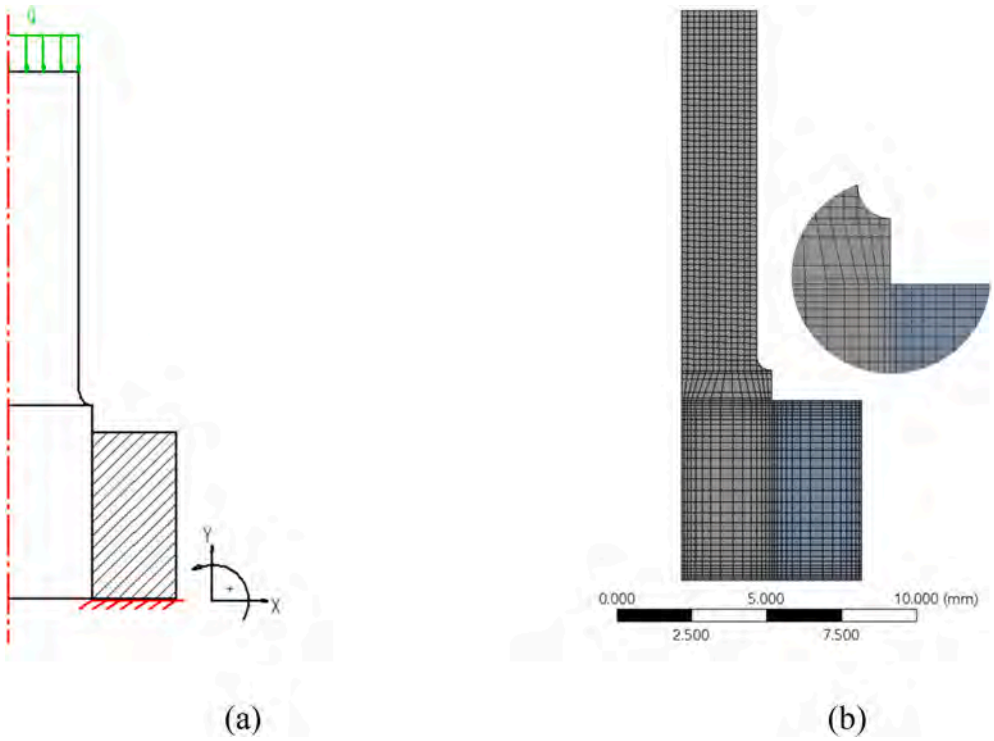

Fig. 19. (a) Boundary conditions of the numerical model; (b) detail of the meshed model.

The material model of both the pin and the collar is a structural steel (E = 200 GPa, $\nu = 0.3$) with a linear elastic behaviour.

As mentioned above, the adhesive behaviour has been modelled by a bilinear traction separation law which assumes an initial linear elastic behaviour followed by linear evolution of damage. The parameters needed to define such behaviour in the Ansys code are the following:

(i) Maximum equivalent tangential contact stress ($T_t^{max} = \tau_{ad}$): this value represents the pure mode II maximum stress. It has been determined based on the outcomes of the experimental tests, according to Eq. (2), where F_{ad} is the joint release force and A is the coupling area of the joint (average values):

$$T_t^{max} = \frac{F_{ad}}{A} = \tau_{ad} \tag{2}$$

(ii) Tangential contact stiffness (Kt): this value represents the linear elastic stiffness of the adhesive layer before damage initiation. It has been calculated as the ratio between the maximum equivalent tangential stress (T_t^{max}) and the corresponding tangential displacement (δ_t^{max}) as average values of the experimental test:

$$K_t = \frac{T_t^{max}}{\delta_t^{max}} \tag{3}$$

(iii) Tangential critical fracture energy (G_{ct}): this value represents the energy absorbed upon failure by the adhesive, hence it is equal to the area under the traction separation curve (tangential stress vs. tangential slip distance). This value has been extrapolated from the literature.

The static test of the epoxy bonded joint has been simulated by means of the FE model described above, in order to evaluate the accuracy of CZM on modelling the pin-collar adhesive joint. According to Eq. (2) and Eq. (3), the preliminary maximum tangential contact stress ($T_{t\ max}$) and stiffness (K_t) have been derived by the results of the present experiment, whereas the tangential critical fracture energy (G_{ct}) has been extrapolated from the literature [44,45] and then it has been fine-tuned to fit the model to the experimental data.

In Fig. 20, the experimental load-displacement curve of the epoxy bonded sample P26, subjected to static loading, (blue solid curve) is compared to the numerical results of two different levels of tuning of the CZM input parameters, hereafter named as realistic (red dashed curve) and unrealistic (purple dashed curve) tuning parameters. The preliminary CZM input parameters were the following: $T_{t\ max} = 35$ MPa, $K_t = 164$ N/mm^3 and $G_{ct} = 7.5$ N/mm. After fine-tuning, the realistic parameters turned out to be $T_{t\ max} = 36.5$ MPa, $K_t = 190$ N/mm^3 and $G_{ct} = 7.5$ N/mm. Tangential stress and stiffness have been incremented by 4% and 16%, respectively, while the fracture energy has undergone no changes. Such modifications to the parameters can be justified in the light of the following remarks: (i) final $T_{t\ max}$ assigned to the CZM is higher than the one estimated by Eq. (2), because the latter oversimplifies the stress distribution along the coupling length as constant while a stress gradient develops at the free edges [23]; (ii) Kt is higher than the experimental value taken from the load displacement curve, because the latter includes the compliance of the adherends. As expected, the force-displacement curve predicted by the numerical model (CZM with realistic parameters) fits the linear part of the experimental curve up to failure, but then it is not able to accurately capture the failure process of the joint, in particular underestimating the absorbed energy. For this reason,

the fracture energy G_{ct} in the CZM unrealistic parameter was incremented up to 42 N/mm in an attempt to predict the second part of the curve. However, an increment of the adhesive fracture toughness of 460%, if compared to the values reported in the literature, is definitely unrealistic, thus suggesting that the representation of a physical phenomenon is missing in the numerical model.

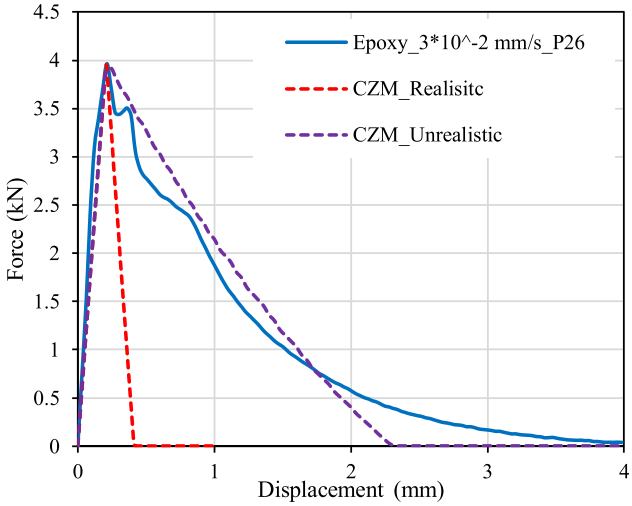

Fig. 20. Experimental force-displacement curve of an epoxy bonded sample vs. two CZM models.

An insight into the missing phenomenon may be derived based on the work by Dragoni and Mauri [49]. They made annular frictional samples reinforced with adhesive, subsequently testing them in torsion, to understand the strength of the hybrid frictional-adhesive joint. By looking at the torque-angle curves they provided, it is quite clear that, after crack initiation, the friction that develops between the crack faces contributes to the global absorbed energy of the joint. Therefore, also in this work, the increment in absorbed energy compared to the one inherent in the adhesive, can be ascribed to friction dissipative phenomena. However, while in Ref. [49] the measured frictional force was constant for the entire test, in the case of adhesive pin collar joints it decreases. As a matter of fact, in the latter, the crack frictional area is reduced during the pin extraction and the radial pressure caused by debris interlocking is not controlled. This results in a high variability of the second portion of the force-displacement curves (see Fig. 20) and makes it difficult to be predicted by numerical simulation.

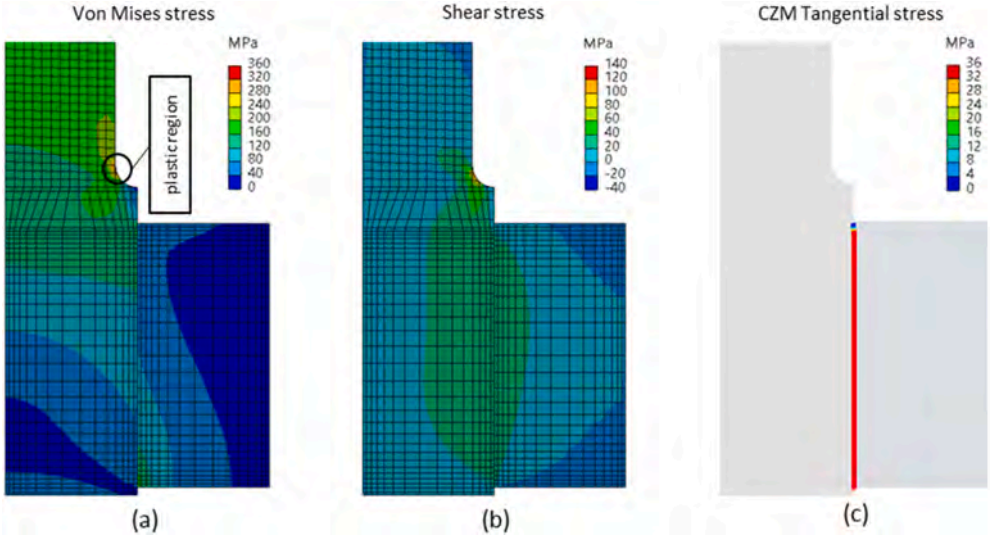

Fig. 21. Stress plots provided by the CZM model at the peak of release force: (a) von-Mises equivalent stress, (b) shear stress, (c) CZM tangential stress.

Fig. 21 shows the von- Mises equivalent stress (a), the shear stress (b) and the CZM tangential stress estimated by the model with the realistic CZM input parameters just before failure (i. e. at the time when the maximum force is reached). Note that the models well estimate the linear portion of the force-displacement curve and hence the results reported in the figure can be considered realistic. It is possible to observe that: (i) there is an equivalent stress peak of 360 MPa at the radiused corner a few millimeters above the upper collar surface. The stress peak overcomes the minimum yield point of the material (290 MPa) but in a very narrow area and therefore it can be neglected; (ii) the shear stress developed on the two adherends near the interfaces and the CZM Tangential stress is evenly distributed over the whole length of the joint.

In summary, the CZM model as conditioned can accurately represent the behaviour of the joint up to fracture initiation, whereas failing to represent the tail of the force-displacement curve which is dominated by frictional phenomena: this point deserves further investigation and will constitute the object of future research.

References

[1] da Silva LFM, Öchsner A, Adams RD, editors. Handbook of adhesion technology. Springer Science & Business Media; 2011.
[2] Adams RD, Comyn J, Wake WC. Structural adhesive joints in engineering. Springer Science & Business Media; 1997.
[3] Croccolo D, De Agostinis M, Vincenzi N. Recent improvements and design formulae applied to front motorbike suspensions. Eng Fail Anal 2010;17(5):1173–87.
[4] Lindholm US. Some experiments with the split Hopkinson pressure bar. J Mech Phys Solid 1964;12:317–35.
[5] Goglio L, Peroni L, Peroni M, Rossetto M. High strain-rate compression and tension behaviour of an epoxy bi-component adhesive. Int J Adhesion Adhes 2008;28:329–39.
[6] Machado JJM, Marques EAS, da Silva, Lucas FM. Adhesives and adhesive joints under impact loadings: an overview. J Adhes 2018;94(6):421–52.
[7] Maurel-Pantel A, Voisin M, Mazerolle F, Lebon F. Comparison of three different adhesive joints using static and dynamic impact tests: development of a new drop weight impact test rig incorporating a modified Arcan fixture. Int J Adhesion Adhes 2022;114:103104.
[8] da Silva LFM, Dillard DA, Blackman B, Adams RD, editors. Testing adhesive joints: best practices. Weinheim, Germany: Wiley-VCH Verlag & Co.; 2012.
[9] You M, Li M-B, Yuan Y-L, Lin G, Ma F-W, Du L-F, Tang S-J. Review of experimental techniques for impact property of adhesive bonds. Int J Adhesion Adhes 2020:102620.
[10] Blackman BRK, Kinloch AJ, Sanchez FR, Teo WS, Williams JG. The fracture behaviour of structural adhesives under high rates of testing. Eng Fract Mech 2009;76(18):2868–89.
[11] Beevers A, Ellis M. Impact behaviour of bonded mild steel lap joints. Int J Adhesion Adhes 1984;4(1):13–6.
[12] Goglio L. In: impact tests. Berlin, Heidelberg: Springer Berlin Heidelberg; 2011. p. 503–32.
[13] Adams RD, editor. Adhesive bonding: science, technology and applications. Cambridge, England: Woodhead Publishing Limited; 2005.
[14] Adams RD, Harris JA. A critical assessment of the block impact test for measuring the impact strength of adhesive bonds. Int J Adhesion Adhes 1996;16:61–71.
[15] ASTM D950-03. Standard test method for impact strength of adhesive bonds. 2011.
[16] Yokoyama T. Experimental determination of impact tensile properties of adhesive butt joints with the split Hopkinson bar. J Strain Anal 2003;38(3):233–45.
[17] Vaidya UK, Gautam ARS, Hosur M, Dutta P. Experimental-numerical studies of transverse impact response of adhesively bonded lap joints in composite structures. Int J Adhesion Adhes 2006;26(3):184–98.
[18] Croccolo D, De Agostinis M, Fini S, Olmi G. Influence of the engagement ratio on the shear strength of an epoxy adhesive by push-out tests on pin-and-collar joints: Part I: campaign at room temperature. Int J Adhesion Adhes 2016;67:69–75.
[19] Croccolo D, De Agostinis M, Fini S, Olmi G, Paiardini L, Robusto F. Influence of the interference level and of the assembly process on the shear strength of Loctite 648 anaerobic adhesive. J Adhes 2020;96(1–4):90–112.
[20] Croccolo D, De Agostinis M, Vincenzi N. Design of hybrid steel-composite interference fitted and adhesively bonded connections. Int J Adhesion Adhes 2012;37:19–25.
[21] Croccolo D, De Agostinis M, Vincenzi N. Static and dynamic strength evaluation of interference fit and adhesively bonded cylindrical joints. Int J Adhesion Adhes 2010;30(5):359–66.
[22] Croccolo D, De Agostinis M, Mauri P. Influence of the assembly process on the shear strength of shaft-hub hybrid joints. Int J Adhesion Adhes 2013;44:174–9.
[23] Croccolo D, De Agostinis M, Fini S, Olmi G. Effect of the engagement ratio and of temperature on the shear strength of epoxy adhesive bonded aluminum alloy pin-and-collar joints. J Adhes 2018;94(11):932–50.
[24] Bezemer AA, Guyt CB, Vlot A. New impact specimen for adhesives: optimization of high-speed-loaded adhesive joints. Int J Adhesion Adhes 1998;18:255–60.
[25] Yokoyama T. Determination of impact shear strength of adhesive joints with the split Hopkinson bar. Key Eng Mater 1998;145–149:317–22.
[26] Yokoyama T, Shimizu H. Evaluation of impact shear strength of adhesive joints with the split Hopkinson bar JSME. Int. J. Ser. A Solid Mech. Mater. Eng. 1998;41:503–9.
[27] Sawa T, Nagai T, Iwamoto T, Kuramoto H. A study on evaluation of impact strength of adhesive joints subjected to impact shear loadings. In: Paper presented at the ASME international mechanical engineering congress and exposition, vol. 15. IMECE; 2008. p. 55–61. Proceedings.
[28] ISO 10123. Adhesives – determination of shear strength of anaerobic adhesives using pin-and-collar specimens. 1990.
[29] ASTM D4562-01. Standard test method for shear strength of adhesives using pin-and-collar specimen. 2013.
[30] EN 10083-2. Steels for quenching and tempering. Part 2: technical delivery conditions for non-alloy steels. 2006.
[31] Henkel Web Site: http://tds.henkel.com/tds5/search.asp?t=648&submit2=Search&Q_PROP7=0&Q_PROP18=0&Q_PROP22=0 (last access April 2022).
[32] Henkel Web Site: htttp://tds.henkel.com/tds5/search.asp?t=9466&submit2=Search&Q_PROP7=0&Q_PROP18=0&Q_PROP22=0 (last access April 2022).
[33] ASTM D7136. Standard test method for measuring the damage resistance of a fiber-reinforced polymer matrix composite to a drop-weight impact event. 2005.
[34] Zarei H, Brugo TM, Belcari J, Bisadi H, Minak G, Zucchelli A. Low velocity impact damage assessment of GLARE fiber-metal laminates interleaved by Nylon 6,6 nanofiber mats. Compos Struct 2017;167:123–31.
[35] Croccolo D, De Agostinis M, Fini S, Olmi G. Influence of the engagement ratio on the shear strength of an epoxy adhesive by push-out tests on pin-and-collar joints: Part II: campaign at different temperature levels. Int J Adhesion Adhes 2016;67:76–85.
[36] da Silva LFM, das Neves PJC, Adams RD, Spelt JK. Analytical models of adhesively bonded joints-part I: literature survey. Int J Adhesion Adhes 2009;29(3):319–30.
[37] da Silva LFM, das Neves PJC, Adams RD, Wang A, Spelt JK. Analytical models of adhesively bonded joints-part II: comparative study. Int J Adhesion Adhes 2009;29(3):331–41.
[38] Öchsner A, Gegner J. Application of the finite element method in the tensile-shear test of adhesive technology. Int J Adhesion Adhes 2001;21:349–53.
[39] Gallio G, Lombardi M, Rovarino D, Fino P, Montanaro L. Influence of the mechanical behaviour of different adhesives on an interference-fit cylindrical joint. Int J Adhesion Adhes 2013;47:63–8.
[40] ISO 4587. Adhesives — determination of tensile lap-shear strength of rigid-to-rigid bonded assemblies. 2003.
[41] He X. A review of finite element analysis of adhesively bonded joints. Int J Adhesion Adhes 2011;31:248–64.
[42] Valente JPA, Campilho RDSG, Marques EAS, Machado JJM, da Silva, Lucas FM. Geometrical optimization of adhesive joints under tensile impact loads using cohesive zone modelling. Int J Adhesion Adhes 2020;97:102492.
[43] May M, Voß H, Hiermaier S. Predictive modelling of damage and failure in adhesively bonded metallic joints using cohesive interface elements. Int J Adhesion Adhes 2014;49:7–17.
[44] Pirondi A, Fersini D, Perotti E, Moroni F. Applicabilità del modello di zona coesiva in simulazioni della frattura per diverse geometrie di giunti incollati. In: Conference proceedings of the IGF19 – Italian group of fracture, milan; 2007. 2-4 July.
[45] Campilho RDSG, Banea MD, Pinto AMG, Da Silva LFM, De Jesus AMP. Strength prediction of single-and double-lap joints by standard and extended finite element modelling. Int J Adhesion Adhes 2011;31(5):363–72.
[46] Alfano G, Crisfield MA. Finite element interface models for the delamination anaylsis of laminated composites: mechanical and computational issues. Int J Numer Methods Eng 2001;50:1701–36.
[47] Turon A, Davila CG, Ponces Camanho P, Costa J. An engineering solution for mesh size effects in the simulation of delamination using cohesive zone models. Eng Fract Mech 2007;74–10:1665–82.
[48] Harper PW, Hallett SR. Cohesive zone length in numerical simulations of composite delamination. Eng Fract Mech 2008;75–16:4774–92.
[49] Dragoni E, Mauri P. Intrinsic static strength of friction interfaces augmented with anaerobic adhesives. Int J Adhesion Adhes 2000;20:315–21.